

# A revisit of generalized scaling of forced turbulence through flux analysis

Wei Zhao

*State Key Laboratory of Photon-Technology in Western China Energy, International Scientific and Technological Cooperation Base of Photoelectric Technology and Functional Materials and Application, Institute of Photonics and Photon-technology, Northwest University, Xi'an 710127, China*

## Abstract

What is the conservative law in the turbulent transport of kinetic energy and scalar variance in wavenumber space is always a focus in the research of turbulence. In this investigation, we theoretically studied the transports of kinetic energy and scalar variance in turbulence (with stratification-like scalar background) driven by a scalar-based volume force, which has a general form as  $M\nabla^\beta s'$  associated with scalar fluctuations  $s'$ , in wavenumber space, relies on flux conservation equation. The equation has one real solution and two complex solutions. The real solution leads to symmetric cascade processes, including inertial subrange (constant fluxes of kinetic energy and scalar variance), CEF subrange (quasi-constant flux of kinetic energy), CSF subrange (quasi-constant flux of scalar variance), and dissipation subrange (nonconstant fluxes of kinetic energy and scalar variance). When  $\beta < 2/3$ , the CEF subrange locates on the lower wavenumber side of the CSF subrange. While  $\beta > 2/3$ , the CEF subrange locates on the higher wavenumber side of the CSF subrange. The scaling exponents in the power spectra of kinetic energy and scalar variance strictly depend on  $\beta$ . In the CEF subrange,  $\xi_u = -5/3$ , while  $\xi_s = -(6\beta + 1)/3$ . In the CSF subrange,  $\xi_u = (4\beta - 11)/5$  and  $\xi_s = -(2\beta + 7)/5$  are both consistent with Zhao and Wang (Journal of Hydrodynamics, 2021, 33(6): 1271-1281). We also systematically studied the cross over wavenumber  $k_{ci}$  between CSF and CEF subrange, and the smallest length scale  $k_k$  in this type of turbulence. The results indicate again  $\beta$  cannot be equal to or larger than 4. The investigations on the 2<sup>nd</sup> solution (a complex solution) of the conservative equations show the symmetry of the cascade process is broken. When  $\beta < 2/3$ , we only observe a new subrange with non-constant  $\Pi_u$  and  $\Pi_s$ , where  $\xi_u = \xi_s = -3$ . However, when  $2/3 < \beta < 4$ , only the CEF subrange is present. For the 3<sup>rd</sup> solution (another complex solution), there is only the CEF subrange in the range  $0 \leq \beta \leq 2.657$ . Beyond this range, the 3<sup>rd</sup> solution becomes physically inappropriate. Thus, a complete transport picture of both kinetic energy and scalar variance has been established for the type of forced turbulence, which unifies stratified turbulence, turbulent thermal convection, electrokinetic turbulence, etc.

## 1. Introduction

How the energy and scalar are transported along with scales in scalar-based forced turbulence are still unsolved problems and might remain far from understanding for a long while. Even in a stratified turbulent thermal convection that has been investigated for over half a century, this problem still remains debated. In the 1950s, Bolgiano (1959) and Obukhov (1959) separately advanced the celebrated BO59 law which can be derived by dimensional analysis on the basis of constant scalar flux of temperate inferred from Benzi et al (1996). The cascade of kinetic energy and temperature variance can both be separated

into a series of subranges from large to small scales in sequence, including large scale injection subrange, buoyancy-driven subrange (in stratified turbulence or turbulent thermal convection (Niemela, Skrbek et al. 2000, Lohse and Xia 2010)), inertial subrange and dissipation subrange etc. In the buoyancy-driven subrange of stably stratified turbulence, the power spectra of velocity and temperature have the following scaling expressions (Davidson 2013, Alam, Guha et al. 2019)

$$E_u(k) \sim \varepsilon_T^{2/5} f_{VB}^{4/5} k^{-11/5} \quad (1.1a)$$

$$E_T(k) \sim \varepsilon_T^{4/5} f_{VB}^{-2/5} k^{-7/5} \quad (1.1b)$$

where  $f_{VB} = \sqrt{\frac{g}{\langle \rho \rangle} \left| \frac{d\rho_0}{dz} \right|}$  is Väisälä–Brunt frequency, with  $\rho_0$ ,  $\langle \rho \rangle$  and  $g$  are background density, mean density with perturbations and gravity respectively. While in the inertial subrange, they got

$$E_u(k) \sim \varepsilon_u^{2/3} k^{-5/3} \quad (1.2a)$$

$$E_T(k) \sim \varepsilon_u^{-1/3} \varepsilon_T k^{-5/3} \quad (1.2b)$$

One essential problem is what the conservative law (or constant quantity) is in the transport of kinetic energy and scalar variance in the scalar-based forced turbulence.

In BO59 law, in the buoyancy-driven subrange, the flux of temperature variance is hypothesized to be constant, while in the inertial subrange, both the fluxes of kinetic energy and temperature variance are constant. The constant flux of scalar variance is also adopted by Zhao and Wang to establish the cascade frameworks of electrokinetic turbulence (Zhao and Wang 2017, Zhao and Wang 2019) and a general form of forced turbulence with  $\nabla^n s$ -type volume forces (Zhao and Wang 2021), where  $s$  is a control scalar for active turbulent transport process. A series of new scaling phenomena, e.g. -7/5 velocity spectrum and -9/5 scalar spectrum have been predicted in electrokinetic turbulence. Nevertheless, the hypothesis of the constant flux of scalar variance results in an unlimited perturbation of flow in small scales when  $n \geq 4$  (Zhao and Wang 2021). The statistical equilibrium system of scalar turbulence is accordingly believed to be collapsed.

However, if we take a look at the inertial subrange, volume-force dominated (VFD) subrange, and the dissipation subrange, it is interesting to find they correspond to constant fluxes of kinetic energy and scalar variance (for inertial subrange), constant flux of scalar variance with nonconstant flux of kinetic energy (VFD subrange), and nonconstant fluxes of kinetic energy and scalar variance. From a sense of symmetry, there should also be a subrange with constant kinetic energy and nonconstant scalar variance, which is yet to be predicted or observed.

In 2019, Alam et al. (2019) revisited BO59 law by combining the flux of kinetic energy and potential energy (which is essentially related to temperature variance). They suggest considering the summation of kinetic energy flux ( $\Pi_u(k)$ ) and temperature variance flux ( $\Pi_T(k)$ ) to be constant, instead of considering each individual to be constant, in the subranges  $k \gg k_\eta$  ( $k_\eta$  is Kolmogorov wavenumber). A -5/3 slope of  $E_u(k)$  was found at the lower wavenumber side of the buoyancy-driven subrange, where the spectra of temperature variance, i.e.  $E_T(k)$ , has a slope of -1/3. In this subrange, only  $\Pi_u(k)$  is approximately constant. Beyond this subrange, the scaling subrange predicted in BO59 law is found numerically, where only  $\Pi_T(k)$  is approximately constant. The existence of the former subrange (-1/3 spectra of  $E_T(k)$ ) is not supported by the previous investigations in stratified turbulence. However, the investigations of Alam et al (2019) is highly inspiring,

as they successfully show the possible existence of constant  $\Pi_u(k)$  subrange and may complete the jigsaw of cascade in scalar-based forced turbulence.

In this investigation, we extend the analysis of Zhao and Wang (2021) and revisit the model of generally forced turbulence with  $\nabla^\beta s'$ -type volume forces, to establish a universal theory for general conservative law in the turbulence with stratification-like scalar background. Besides the influence of derivation order  $\beta$ , we also take the selection of conservative equation solutions into account. Rich information of characteristic microscales has been provided accordingly.

## 2. Theory

In this investigation, we revisit a general model on scalar-based forced turbulence (Zhao and Wang 2021) with stratified scalar features, by analogy with the analytical method of Alam et al (2019). The turbulent model can be dominated by the following equations

$$\frac{D\mathbf{u}}{Dt} = -\frac{1}{\rho} \nabla p + \nu \nabla^2 \mathbf{u} + \mathbf{M} \nabla^\beta s' \quad (2.1a)$$

$$\frac{D s'}{Dt} = -\mathbf{N} \cdot \mathbf{u} + D_s \nabla^2 s' \quad (2.1b)$$

$$\nabla \cdot \mathbf{u} = 0 \quad (2.1c)$$

where  $\rho$  is the fluid density,  $\mathbf{u}$  denotes velocity vector,  $p$  is pressure,  $s'$  is any scalar fluctuations that control the volume force,  $\mathbf{M}$  denotes a certain dimensional vector associated with the physical field,  $\nabla^\beta s'$  is a scalar function associated with a specific  $\beta^{\text{th}}$ -order derivative of the scalar  $s'$ ,  $\mathbf{N}$  is a vector related to scalar  $s$  to characterize the feature of stratified scalar background, and  $\nu$  and  $D_s$  are the kinematic viscosity and diffusivity of the scalar respectively. For stratified thermal convection, let  $s' = \rho' g f_{VB}^{-1} \langle \rho \rangle^{-1}$  being density fluctuations,  $\beta = 0$ ,  $\mathbf{M} = \mathbf{N} = -f_{VB} \hat{\mathbf{z}}$ , the control equations (2.1a-b) are consistent with Alam et al. (2019). For stratified electrokinetic turbulence, we can let  $\beta = 1$ ,  $\mathbf{M} = -\varepsilon E^2 \hat{\mathbf{y}} / \rho \langle \sigma \rangle$ ,  $\mathbf{N} = \nabla \langle \sigma \rangle$ , where  $\sigma$  is electric conductivity,  $E$  is electric field in  $y$ -direction ( $\hat{\mathbf{y}}$ ) that perpendicular to initial interface of electric conductivity (Wang, Yang et al. 2014, Wang, Yang et al. 2016). For one-dimensional spectra, according to Verma (2004, Verma 2018)

$$E_u(k)dk = \sum_{k < |k'| \leq k + dk} \frac{1}{2} |u(\mathbf{k}')|^2 \quad (2.2a)$$

$$E_s(k)dk = \sum_{k < |k'| \leq k + dk} \frac{1}{2} |s'(\mathbf{k}')|^2 \quad (2.2b)$$

$$\Pi_u(k_0) = \sum_{|k| > k_0} \sum_{|m| \leq k_0} \text{Im}\{[\mathbf{k} \cdot \mathbf{u}(\mathbf{n})][\mathbf{u}(\mathbf{m}) \cdot \mathbf{u}^*(\mathbf{k})]\} \quad (2.2c)$$

$$\Pi_s(k_0) = \sum_{|k| > k_0} \sum_{|m| \leq k_0} \text{Im}\{[\mathbf{k} \cdot \mathbf{u}(\mathbf{n})][s'(m)s'^*(k)]\} \quad (2.2d)$$

where  $E_u(k)$  is kinetic energy spectrum,  $E_s(k)$  is scalar energy spectrum,  $\Pi_u(k_0)$  and  $\Pi_s(k_0)$  are the fluxes of kinetic energy and scalar variance in spectral space respectively.  $k = m + n$ . Let  $E_u(\mathbf{k}) = \frac{1}{2} |\mathbf{u}(\mathbf{k})|^2$  and  $E_s(\mathbf{k}) = \frac{1}{2} |s'(\mathbf{k})|^2$ , if we consider the contribution of scalar-based volume force (SVF) to scalar transport, under statistical equilibrium state, we have (Davidson 2013, Alam, Guha et al. 2019)

$$T_u(\mathbf{k}) + F_s(\mathbf{k}) - D_u(\mathbf{k}) = 0 \quad (2.3a)$$

$$T_s(\mathbf{k}) - F_A(\mathbf{k}) - D_s(\mathbf{k}) = 0 \quad (2.3b)$$

$T_u(\mathbf{k})$  and  $D_u(\mathbf{k})$  are the nonlinear kinetic energy transfer rate and dissipation rate, respectively.  $T_s(\mathbf{k})$  and  $D_s(\mathbf{k})$  are the nonlinear transfer rate of scalar variance and scalar

dissipation rate, respectively.  $F_s(\mathbf{k})$  denotes the energy feeding rate by SVF and  $F_A(\mathbf{k})$  is the scalar feeding rate by bulk components. These quantities can be expressed as

$$T_u(\mathbf{k}) = \sum_m \text{Im}\{[\mathbf{k} \cdot \mathbf{u}(\mathbf{n})][\mathbf{u}(\mathbf{m}) \cdot \mathbf{u}^*(\mathbf{k})]\} \quad (2.4a)$$

$$T_s(\mathbf{k}) = \sum_m \text{Im}\{[\mathbf{k} \cdot \mathbf{u}(\mathbf{n})][s'(\mathbf{m})s'^*(\mathbf{k})]\} \quad (2.4b)$$

$$F_s(\mathbf{k}) = M\text{Re}[(\nabla^\beta s')(\mathbf{k}) \cdot \mathbf{u}^*(\mathbf{k})] = M\text{Re}[s'(\mathbf{k})\mathbf{k}^\beta \cdot \mathbf{u}^*(\mathbf{k})] \quad (2.4c)$$

$$F_A(\mathbf{k}) = N\text{Re}[s'(\mathbf{k}) \cdot \mathbf{u}^*(\mathbf{k})] = N\text{Re}[s'(\mathbf{k}) \cdot \mathbf{u}^*(\mathbf{k})] \quad (2.4d)$$

$$D_u(\mathbf{k}) = 2\nu k^2 E_u(\mathbf{k}) \quad (2.4e)$$

$$D_s(\mathbf{k}) = 2D_s k^2 E_s(\mathbf{k}) \quad (2.4f)$$

where  $M = |\mathbf{M}|$  and  $N = |\mathbf{N}|$  denote the magnitudes respectively. Combining Eqs. (2.2a-b) with (2.4a-b), it is obtained,

$$\Pi_u(k_0) = -\sum_{|\mathbf{k}| \leq k_0} T_u(\mathbf{k}), \Pi_s(k_0) = \sum_{|\mathbf{k}| \leq k_0} T_s(\mathbf{k}) \quad (2.5)$$

After applying similar mathematical processing according to Alam et al. (2019), we have

$$0 = -\frac{d}{dk} \Pi_u(k) + F_s(k) - D_u(k) \quad (2.6a)$$

$$0 = -\frac{d}{dk} \Pi_s(k) - F_A(k) - D_s(k) \quad (2.6a)$$

where

$$F_s(k)dk = \sum_{k < |\mathbf{k}'| \leq k + dk} M\text{Re}[s'(\mathbf{k}')\mathbf{k}'^\beta \cdot \mathbf{u}^*(\mathbf{k}')] \quad (2.7a)$$

$$F_A(k)dk = \sum_{k < |\mathbf{k}'| \leq k + dk} N\text{Re}[s'(\mathbf{k}') \cdot \mathbf{u}^*(\mathbf{k}')] \quad (2.7b)$$

$$D_u(k)dk = 2\nu \sum_{k < |\mathbf{k}'| \leq k + dk} k'^2 E_u(\mathbf{k}') \quad (2.7c)$$

$$D_s(k)dk = 2D_s \sum_{k < |\mathbf{k}'| \leq k + dk} k'^2 E_s(\mathbf{k}') \quad (2.7d)$$

When  $dk \rightarrow 0$ , it is approximately having

$$F_s(k) = M\text{Re}[s'(k)\mathbf{k}^\beta \cdot \mathbf{u}^*(\mathbf{k})] \quad (2.8a)$$

$$F_A(k) = N\text{Re}[s'(k) \cdot \mathbf{u}^*(\mathbf{k})] \quad (2.8b)$$

$$D_u(k) = 2\nu k'^2 E_u(\mathbf{k}) \quad (2.8c)$$

$$D_s(k) = 2D_s k'^2 E_s(\mathbf{k}) \quad (2.8d)$$

In the inertial subrange, where the influence of forcing and dissipation is negligible, we have

$$\frac{d}{dk} \Pi_u(k) = 0 \quad (2.9a)$$

$$\frac{d}{dk} \Pi_s(k) = 0 \quad (2.9b)$$

Or

$$\Pi_u(k) = \text{const along } k \quad (2.10a)$$

$$\Pi_s(k) = \text{const along } k \quad (2.10b)$$

The inertial subrange must have constant  $\Pi_u$  and  $\Pi_s$ . This is a special solution of Eq. (2.12) as can be seen later.

In the VFD subrange, the dissipation terms of kinetic energy and scalar variance are ignored, whereas

$$\frac{d}{dk} \Pi_u(k) = F_s(k) \quad (2.11a)$$

$$\frac{d}{dk} \Pi_s(k) = -F_A(k) \quad (2.11b)$$

Thus, from Eqs. (2.8a-b) and (2.11a-b), easily we get

$$F_s(k) - \frac{M}{N} F_A(k) k^\beta = 0 = \frac{d}{dk} \Pi_u(k) + \frac{M}{N} k^\beta \frac{d}{dk} \Pi_s(k) \quad (2.12)$$

According to Alam et al (2019),

$$E_u(k) = u_k^2/k \quad (2.13a)$$

$$E_s(k) = s_k^2/k \quad (2.13b)$$

$$\Pi_u(k) = k u_k^3 \quad (2.13c)$$

$$\Pi_s(k) = k s_k^2 u_k \quad (2.13d)$$

Substituting  $\Pi_u(k)$  and  $\Pi_s(k)$  into the Eq. (2.12) above,

$$\frac{d}{dk} k u_k^3 + \frac{M}{N} k^\beta \frac{d}{dk} k s_k^2 u_k = 0 \quad (2.14)$$

When  $\beta = 0$  and  $M = N = -f_{VB}$ , Eq. (2.14) is equivalent to Eq. (2.15) in the manuscript of Alam et al. (2019) for stratified turbulence. Considering in VFD subrange, the flow is driven by the  $M \nabla^\beta s'$  type volume force, dimensionally  $k u_k^2 = k^\beta M s_k$ , then Eq. (2.14) becomes

$$u_k + \frac{(3-2\beta)}{MN} k^{2-3\beta} u_k^3 + \left(3k + \frac{5}{MN} k^{3-3\beta} u_k^2\right) \frac{du_k}{dk} = 0 \quad (2.15)$$

Eq. (2.15) is a universal equation for forced turbulence driven by the  $M \nabla^\beta s'$  type volume force. There are three solutions of Eq. (2.15), including one real solution and two complex solutions. Here, all the three solutions are taken into account, say  $u_{k,i}^2 = u_{k,i} \cdot u_{k,i}^*$  with  $u_{k,i}^*$  being the complex conjugate of  $u_{k,i}$  which is the  $i$ th solution of Eq. (2.15). Thus, we can simply have

$$E_u(k) = k^{-1} (u_k \cdot u_k^*) \sim k^{\xi_u} \quad (2.16a)$$

$$E_s(k) = \frac{s_k^2}{k} = \left( \frac{k u_k^2}{k^\beta M} \right)^2 k^{-1} = \left( \frac{k^2 E_u(k)}{k^\beta M} \right)^2 k^{-1} = M^{-2} k^{3-2\beta} E_u^2(k) \sim k^{\xi_s} \quad (2.16b)$$

$$\Pi_u(k) = k u_k^3 = k (k E_u(k))^{3/2} = k^{5/2} E_u^{3/2}(k) \sim k^{\lambda_u} \quad (2.16c)$$

$$\Pi_s(k) = k s_k^2 u_k = k^2 E_s(k) [k^{1/2} E_u^{1/2}(k)] = M^{-2} k^{\frac{11}{2}-2\beta} E_u^{5/2}(k) \sim k^{\lambda_s} \quad (2.16d)$$

where  $\xi_u, \xi_s, \lambda_u, \lambda_s$  denote the scaling exponents of  $E_u, E_s, \Pi_u$  and  $\Pi_s$  respectively.

### 3. Numerical results

It can be solved numerically after settling  $\beta, M$  and  $N$ . In this investigation, we used a simple forward wind scheme to solve Eq. (2.15), i.e.

$$u_{k,i,m} + \frac{(3-2\beta)}{MN} k_m^{2-3\beta} u_{k,i,m}^3 + \left(3k + \frac{5}{MN} k_m^{3-3\beta} u_{k,i,m}^2\right) \frac{u_{k,i,m} - u_{k,i,m-1}}{k_m - k_{m-1}} = 0 \quad (3.1)$$

for  $m = 2, 3, \dots, m_{max}$ , where  $m_{max}$  is the maximum index of wavenumber in this investigation.  $u_{k,i,m}(k_m)$  denotes the  $u_{k,i}$  at  $k_m$ . Apparently, the solution of Eq. (3.1) relies on an initial  $u_{k,i}$  at  $k_1$ , i.e.  $u_{k,i,1}$ . Considering the total kinetic energy  $\int E_u(k)dk$  is inevitably determined by  $MN$ , the distribution of  $u_k$ , including  $u_{k,i,1}$ , relies on  $MN$  as well. The influence of  $\beta$ ,  $MN$ ,  $u_{k,i}$  and the initial value  $u_{k,i,1}$  will be comprehensively discussed in the following sections.

### 3.1 Influence of $\beta$

According to Eq. (2.15), it is explicitly seen that  $\beta$  is a crucial parameter in determining the transport of kinetic energy and scalar variance. Zhao and Wang (2021) theoretically predicted that  $\beta$  should be smaller than 4, otherwise, the statistical equilibrium of the system can be broken, as a result of unlimited accumulation of energy at small scales. Although the conclusion is attributed to constant flux of scalar variance which could be inaccurate at high wavenumber, this restriction (i.e.  $\beta < 4$ ) is still applicable as discussed in section 3.2.

Generally, two additional subranges can be observed in the VFD subrange (Figure 1): One has a quasi-constant flux of kinetic energy (say “CEF” subrange), the other has a quasi-constant flux of scalar variance (say “CSF” subrange). The two subranges intersect with each other at a critical wavenumber  $k_{ci}$ .

#### (1) CEF subrange

Figure 1(a) shows the variation of  $E_u(k)$  versus  $\beta$  in a large wavenumber range. When  $\beta < 2/3$ , the CEF subrange locates at lower wavenumber range, i.e.  $k \ll k_{ci}$ . The corresponding  $\xi_u = -5/3$  which is the same as that in the inertial subrange. However, when  $\beta > 2/3$ , the CEF subrange moves to the higher wavenumber range, i.e.  $k \gg k_{ci}$ . In the CEF subrange, the flux of kinetic energy is quasi-constant, as shown in Figure 1(c). However, it should be noted that the reason we call it “quasi-constant” is  $\Pi_u$  is not precisely constant. There exists a very small ( $\sim 1/30$  or smaller) slope of  $\Pi_u$  in the CEF subrange of Figure 1(c). This explains why  $\Pi_s$  can be non-constant (Figure 1(d)) according to Eq. (2.12).

In the CEF subrange,  $E_s(k)$  shows a new scaling behaviour that has never been predicted. As plotted in Figure 1(b) and Figure 2,  $\xi_s$  has the following expression

$$\xi_s = -(6\beta + 1)/3 \quad (3.2)$$

To the best of the author’s knowledge, this scaling law has not been predicted by other theoretical analyses or numerical simulations. However, this law is consistent with the recent observation in electrokinetic turbulence ( $\beta = 1$ ) where a  $-7/3$  slope of concentration spectra has been experimentally observed (discussed in another manuscript). The limited results partially support the analytical method in this investigation. In the CEF subrange, the flux of scalar variance has a scaling exponent as

$$\lambda_s = (4 - 6\beta)/3 \quad (3.3)$$

When  $\beta < 2/3$ , an increasing  $\Pi_s$  with  $k$  can be predicted in the CEF subrange. However, when  $\beta > 2/3$ ,  $\lambda_s$  becomes negative and accordingly,  $\Pi_s$  decreases with  $k$  rapidly. In other words, the transport rate of scalar variance towards a small scale can be inhibited. In CEF subrange, since  $E_u \sim k^{-5/3}$  and  $E_s \sim k^{-(6\beta+1)/3}$ , thus according to Eqs. (2.8a-b),  $F_s(k) \sim k^{-1}$  and  $F_A(k) \sim k^{-\beta-1}$ .

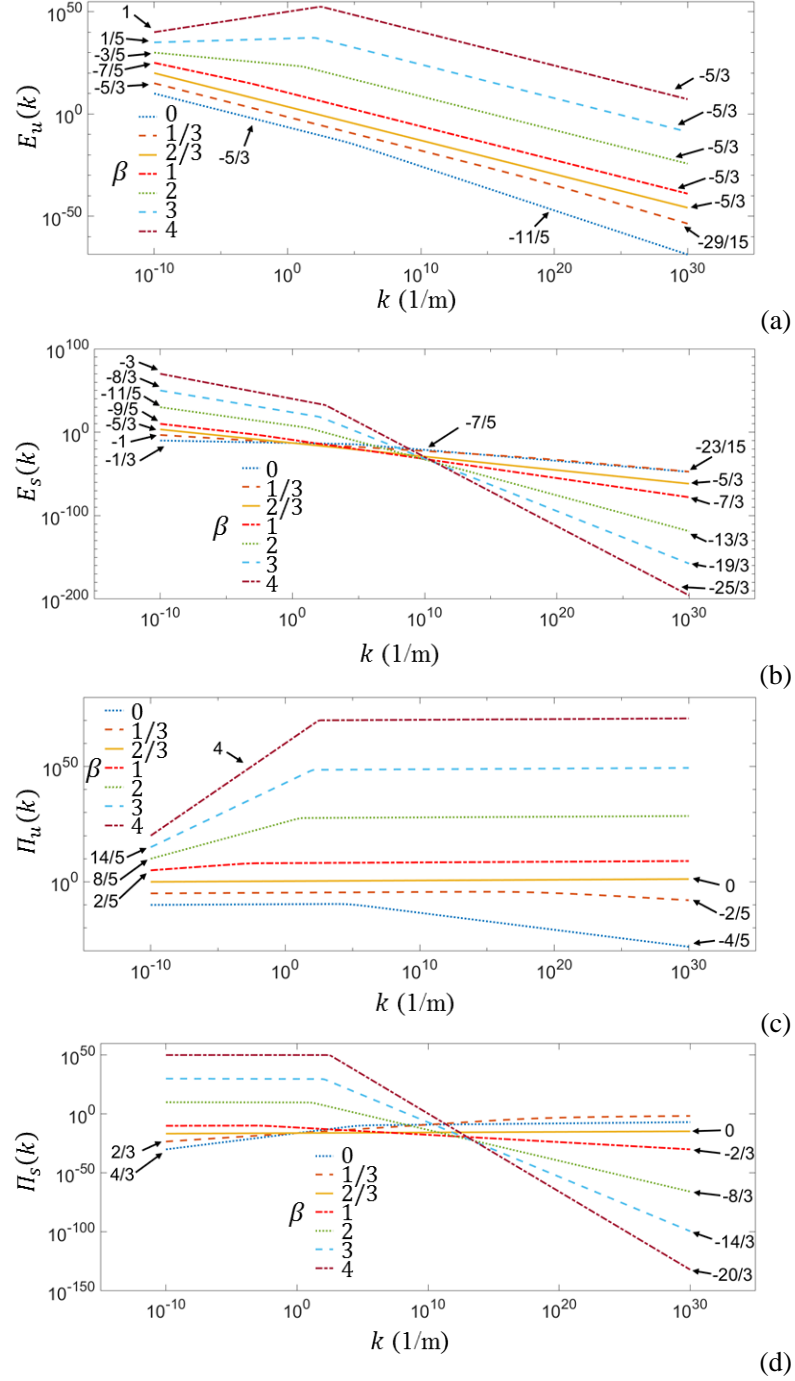


Figure 1. Influence of  $\beta$ , where  $M = N = 1$ , and only the first solution (real solution), i.e.  $u_{k,1}$ , has been taken into account. The initial value  $u_{k,1,1} = 1$ . (a) Power spectra of kinetic energy  $E_u$ . Each curve has been shifted by  $10^5$  vertically. (b) Power spectra of scalar variance  $E_s$ . (c) Flux of kinetic energy  $\Pi_u$ . Each curve has been shifted by  $10^5$  vertically. (d) Flux of scalar variance  $\Pi_s$ .

## (2) CSF subrange

In the CSF subrange, as shown in Figure 1(d), when  $\beta < 2/3$ , the CSF subrange locates at the higher wavenumber range of CEF subrange, i.e.  $k \gg k_{ci}$ . However, when  $\beta > 2/3$ , the CSF subrange moves to the lower wavenumber range of CEF subrange, i.e.  $k \ll k_{ci}$ . From the numerical calculation, it is found  $\xi_u$  in CSF subrange follows the equations below

$$\xi_u = (4\beta - 11)/5 \quad (3.4)$$

This is explicitly consistent with the theory of Zhao and Wang (2021), where they assume  $\Pi_s(k)$  is constant has also been supported by Figure 1(d). The corresponding scaling exponents of  $\Pi_u(k)$  becomes

$$\lambda_u = (6\beta - 4)/5 \quad (3.5)$$

This is consistent with Figure 1(c). It again indicates in the CSF subrange,  $\Pi_s(k)$  is quasi-constant, with a small slope ( $\sim 1/10$ ). As shown in Figure 1(b) and Figure 2,  $\xi_s$  is also consistent with the predictions by Zhao and Wang (2021), i.e.

$$\xi_s = -(2\beta + 7)/5 \quad (3.6)$$

In CSF subrange, since  $E_u \sim k^{(4\beta-11)/5}$  and  $E_s \sim k^{-(2\beta+7)/5}$ , according to Eqs. (2.8a-b), we have  $F_s(k) \sim k^{(6\beta-9)/5}$  and  $F_A(k) \sim k^{(\beta-9)/5}$ .

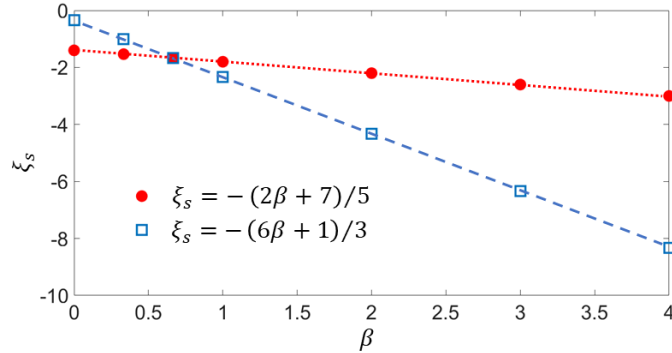


Figure 2. Scaling exponents of  $E_s$ , i.e.  $\xi_s$ , in different subranges of wavenumber. The red dots represent the CSF subrange, while the blue squares represent the CEF subrange.

## (3) Special case at $\beta = 2/3$

From Figure 1, it is interesting to see,  $\beta = 2/3$  is a very special value under which  $\xi_u = \xi_s = -5/3$  and  $\lambda_u = \lambda_s = 0$ . This means, at this  $\beta$ , there exists a delicate balance among the volume force, the transport of kinetic energy and scalar variance, which makes both kinetic energy and scalar variance experience inertial cascades from large to small scales. This result can be predicted if we rewrite Eq. (2.12) as  $\frac{d}{dk} \Pi_u(k) + \frac{M}{N} k^\beta \frac{d}{dk} \Pi_s(k) = \frac{d}{dk} \Pi_u(k) + \frac{1}{MN} k^\beta \frac{d}{dk} \left[ k^{\frac{4}{3}-2\beta} \Pi_u(k)^{\frac{5}{3}} \right] = 0$ . To make the equation established, we need both  $\Pi_u(k) = \text{const}$  and  $k^{\frac{4}{3}-2\beta} = \text{const}$  in the VFD subrange. Accordingly,  $\beta = 2/3$ . The result indicates, on one hand, direct observations of constant fluxes of kinetic energy and scalar variance, and the corresponding  $-5/3$  slopes in the spectra of kinetic energy and scalar

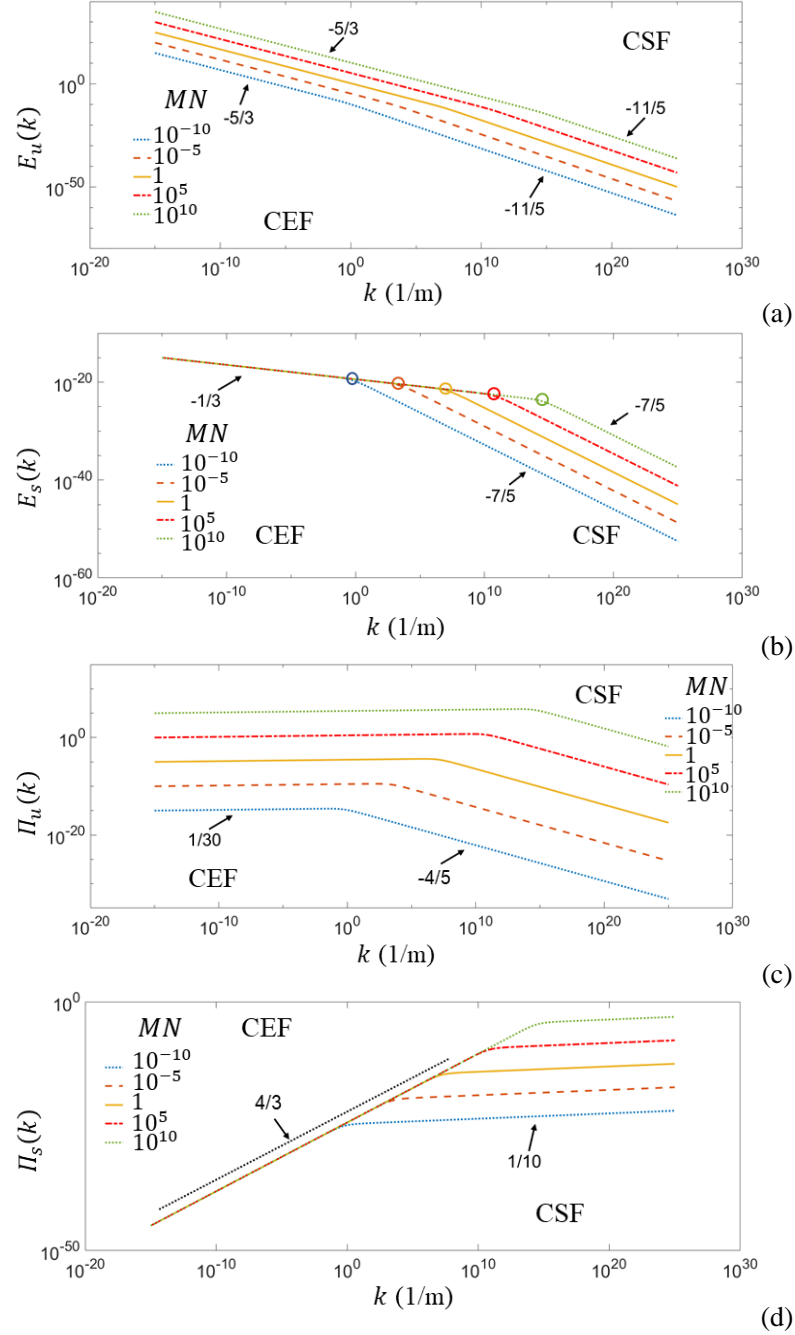


Figure 3 Influence of  $N$ , where  $\beta = 0$ . Here, only the first solution (real solution), i.e.  $u_{k,1}$ , has been taken into account. The initial value  $u_{k,1,1} = 1$ . (a) Power spectra of kinetic energy  $E_u$ . Each curve has been shifted by  $10^5$  vertically. (b) Power spectra of scalar variance  $E_s$ . The colour circles denote the position of  $k_{ci}$ . (c) Flux of kinetic energy  $\Pi_u$ . Each curve has been shifted by  $10^5$  vertically. (d) Flux of scalar variance  $\Pi_s$ .

variance, are insufficient to ensure the existence of K41 law (Kolmogorov 1941, Frisch 1995) and Obukhov-Corrsin law (Obukhov 1949, Corrsin 1951) in forced turbulence. On the other hand, it is possible to generate forced turbulence with  $\beta = 2/3$  to significantly extend the wide of the  $-5/3$  scaling subrange by combining the conventional inertial subrange and the VFD subrange.

### 3.2 Influence of the magnitude of $MN$

According to Eq. (2.15),  $M$  and  $N$  has no difference in the scaling behaviour of  $u_k$  and the related quantities. However,  $M$  does affect the magnitudes of  $E_s(k)$  and  $\Pi_s$  from Eqs. (2.16b) and (2.16d). For better comparison, we change the magnitude of  $MN$  through  $N$ , and keep  $M = 1$  unchanged.

(i) When  $\beta = 0$ , from Figure 3(a), it can be seen in the CEF subrange,  $\xi_u = -5/3$ , while in the CSF subrange,  $\xi_u = -11/5$ . The corresponding  $\xi_s$  in these two subranges are  $-1/3$  and  $-7/5$  respectively. All these data are consistent with the investigations of Alam et al (2019). However, a close view on  $\Pi_u(k)$  and  $\Pi_s(k)$  reveal the “quasi-constant” feature of the two subranges. In CEF subrange,  $\Pi_u(k)$  have very small slopes of  $1/30$  which is nearly zero. While in the CSF subrange,  $\Pi_s(k)$  have slopes of  $1/10$ . Although  $\xi_s$  in CSF subrange is not exactly zero, the  $\xi_u$  calculated (Figure 3(a)) is still consistent with BO59 law. Therefore, we can roughly ignore the influence of the slightly inclining  $\Pi_u(k)$  and  $\Pi_s(k)$  in CEF and CSF subranges respectively. In the CEF subrange,  $\lambda_s = 4/3$ . While in the CSF subrange,  $\lambda_u = -4/5$ . These two scaling exponents of  $\Pi_u(k)$  and  $\Pi_s(k)$  are sufficiently close to Eq. (3.3) and (3.5) respectively.

As  $MN$  is increased, we can see the critical wavenumber  $k_{ci}$  increases rapidly (see Figure 3(b) as an example), which indicates the CEF subrange invades the CSF subrange and push it towards the higher wavenumber region. There is also no cross over observed between the VFD subrange and inertial subrange. Alam et al (2019) attributed the absence of inertial subrange to the insufficient strong disturbing from buoyancy.

(ii) As  $\beta$  is increased to 2, from Figure 4(a), the CEF subrange moves to the right side of the CSF subrange, where  $\xi_u = -5/3$  in the CEF subrange and  $\xi_u = -3/5$  in the CSF subrange. The corresponding  $\xi_s$  in these two subranges are  $-13/3$  and  $-11/5$  respectively (Figure 4(b)). In the CEF subrange,  $\lambda_u = 1/30$  is pretty close to zero from the  $\Pi_u$  plot in Figure 4(c). While in the CSF subrange,  $\Pi_s$  are exactly flat with  $\lambda_u$  equal to zero, as shown in Figure 4(d). Furthermore,  $\lambda_u = 8/5$  in the CSF subrange, and  $\lambda_s = -8/3$  in the CEF subrange. All the scaling exponents of  $\Pi_u$  and  $\Pi_s$  are exactly consistent with Eq. (3.5) and (3.3) respectively. Basically, as  $\beta$  is increased,  $\lambda_u$  and  $\lambda_s$  become closer to Eq. (3.5) and (3.3) respectively.

In this case, when  $MN$  is increased, we can see the critical wavenumber  $k_{ci}$  decreases (see Figure 4(c) as an example) in a much slower manner than that of  $\beta = 0$ . The CEF subrange pushes the CSF subrange towards the lower wavenumber region, takes over the detectable wavenumber region and moves the CSF subrange out of the detectable wavenumber region. There is also no cross over observed between the VFD subrange and inertial subrange.

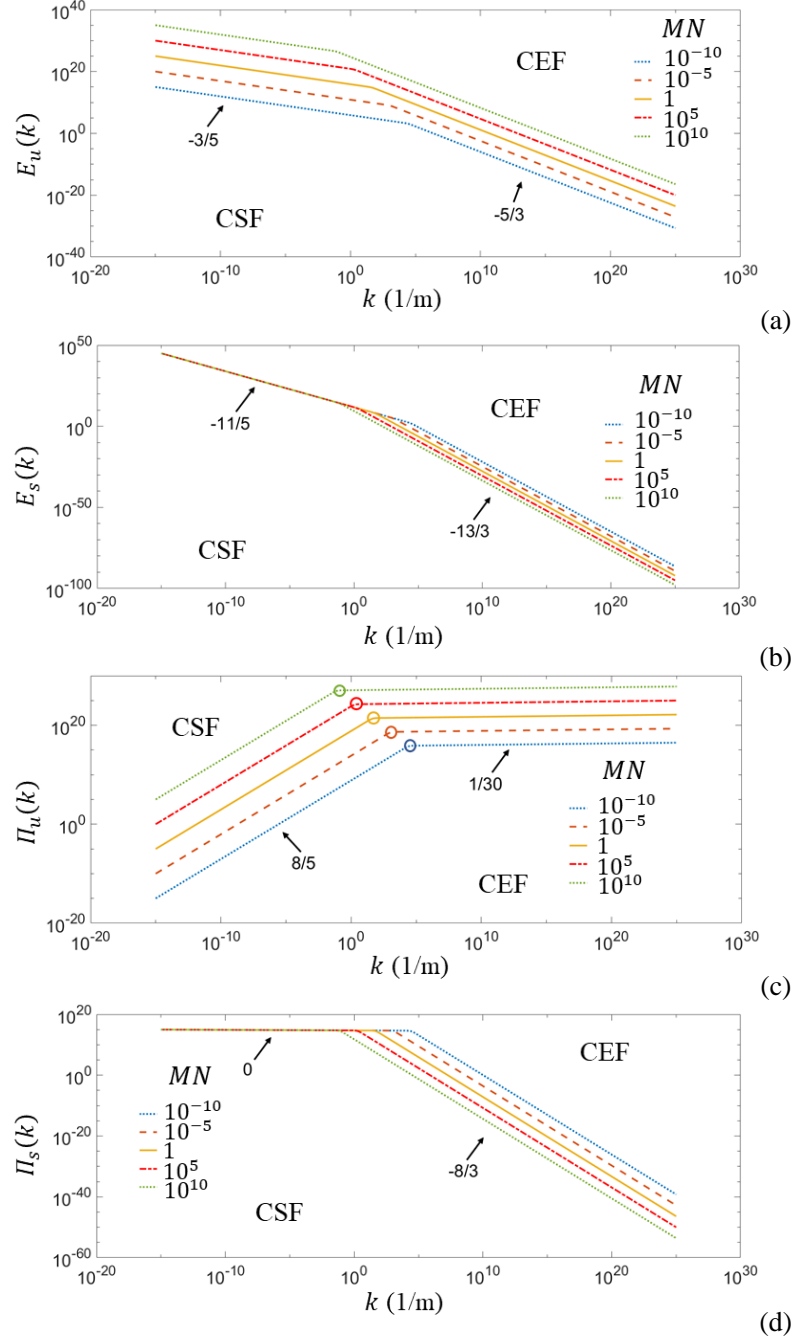


Figure 4 Influence of  $N$ , where  $\beta = 2$ . Here, only the first solution (real solution), i.e.  $u_{k,1,1} = 1$ . (a) Power spectra of kinetic energy  $E_u$ . Each curve has been shifted by  $10^5$  vertically. (b) Power spectra of scalar variance  $E_s$ . (c) Flux of kinetic energy  $\Pi_u$ . Each curve has been shifted by  $10^5$  vertically. The colour circles denote the position of  $k_{ci}$ . (d) Flux of scalar variance  $\Pi_s$ .

(iii) The critical wavenumber  $k_{ci}$  has been investigated for different  $\beta$  and  $u_{k,1,1}$  in this section. The influence of  $\beta$  on  $MN \sim k_{ci}$  relationship has been plotted in Figure 5(a). In the log-log plot, all the  $MN \sim k_{ci}$  curves exhibit a linear relationship, which indicates  $k_{ci} \sim (MN)^\varphi$ , where  $\varphi = \varphi(\beta)$  has been plotted in the inset of Figure 5(a). As  $\beta$  is increased from 0 to 3,  $\varphi$  first decreases from 0.73 (at  $\beta = 0$ ) to -0.71 (at  $\beta = 1$ ), then it slightly increase to -0.17 at  $\beta = 3$ . A positive  $\varphi$  means  $k_{ci}$  increases with  $MN$ , while a negative one means  $k_{ci}$  decreases with  $MN$ . However, this is counterintuitive and conflicts with experimental results, e.g. in EK turbulence where  $\beta = 1$ . The reason is attributed to the neglecting influence of  $u_{k,1,1}$ .

In the investigation above, we fixed  $u_{k,1,1} = 1$  to evaluate the influence of  $MN$ . Nevertheless, when  $MN$  is changed in practice,  $u_{k,1,1}$  which is related to  $E_u$  and  $E_s$  at large scale should also be changed accordingly. Or in other words,  $u_{k,1,1}$  is a function of  $MN$ . We study the influence of  $u_{k,1,1}$  selected for numerical simulation on  $k_{ci}$ . It is found that  $k_{ci}$  changes with  $u_{k,1,1}$  as  $k_{ci} \sim u_{k,1,1}^\psi$ , with  $\psi = \psi(\beta)$  plotted in the inset of Figure 5(b). Relative to that of  $MN$ ,  $k_{ci}$  changes faster with  $u_{k,1,1}$  as indicated by the larger magnitude of  $\psi$ . At  $\beta = 0$ ,  $\psi = -1.49$ , indicating  $k_{ci}$  decreases with  $u_{k,1,1}$ . When  $\beta = 1$ ,  $\psi$  is increased to 1.44 which indicates  $k_{ci}$  increases with  $u_{k,1,1}$ . As  $\beta$  is further increased to 3,  $\psi$  again decreases to 0.34.

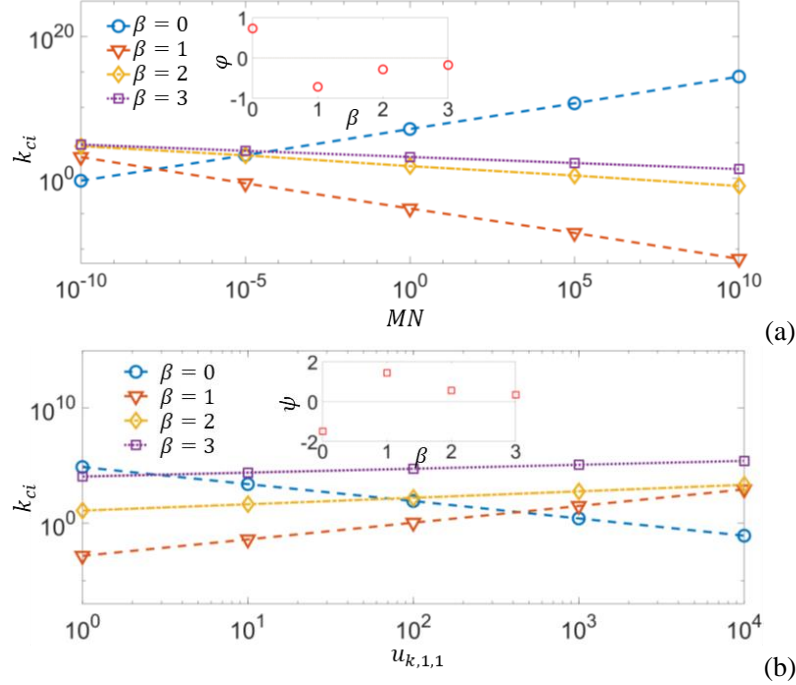


Figure 5 Critical wavenumber  $k_{ci}$  varies with  $MN$  and  $u_{k,1,1}$  for different  $\beta$ . (a)  $k_{ci}$  vs  $MN$  at  $u_{k,1,1} = 1$ . The inset shows the relation between  $\varphi$  and  $\beta$ . (b)  $k_{ci}$  vs  $u_{k,1,1}$  at  $M = N = 1$ . The inset shows the relation between  $\psi$  and  $\beta$ .

After taking the influence of both  $MN$  and  $u_{k,1,1}$  into account, we have  $k_{ci} \sim (MN)^\varphi u_{k,1,1}^\psi$ . The direct relationship between  $u_{k,1,1}$  and  $MN$  relies on the physical problem and the dynamic system. It can be determined if the relation between  $k_{ci}$  and  $MN$  (or the related dimensionless parameters, e.g. Richardson number or Froude number in

stratified turbulence (Maffioli and Davidson 2016, Howland, Taylor et al. 2020, Okino and Hanazaki 2020)) is evaluated through either experiments or numerical simulations.

**(iv)** Furthermore, when  $\beta > 2/3$ , the kinetic energy has constant flux in the CEF subrange in the high wavenumber region where the scalar flux is decreasing with  $k$ . The kinetic energy is subsequently dissipated in the dissipation subrange. Therefore, there must be another cross over wavenumber  $k_k$  which connects the CEF subrange and the dissipation subrange, and functionalizes similarly to the Kolmogorov wavenumber  $k_\eta$  in free turbulence. To determine  $k_k$ , the following two conditions must be satisfied simultaneously

$$\begin{cases} F_s(k_k) = D_u(k_k) \\ F_A(k_k) = D_s(k_k) \end{cases} \quad (3.7)$$

After simple mathematical processing, the equations are further converted to

$$\begin{cases} M[E_s^{1/2}(k_k)E_u^{-1/2}(k_k)k_k^{\beta-2}] = 2\nu \\ N[E_s^{-1/2}(k_k)E_u^{1/2}(k_k)k_k^{-2}] = 2D_s \end{cases} \quad (3.8)$$

which leads to

$$k_k = \left(\frac{MN}{4\nu D_s}\right)^{\frac{1}{4-\beta}} \quad (3.9)$$

Interestingly, we can see a singularity emerges at  $\beta = 4$ . When  $\beta$  is over 4, the exponent becomes negative and  $k_k$  becomes increases with  $\nu$  and  $D_s$ . This is unreasonable in physics since a smaller  $\nu$  should provide a larger  $k_k$ . Thus, we have to claim that  $\beta < 4$  in an equilibrium system again. This is surprisingly coincident with Zhao and Wang (2021). For instance, in EK turbulence where  $\beta = 1$ ,  $M = \varepsilon E^2 / \rho \langle \sigma \rangle$  and  $N = \Delta \sigma / L$ ,  $k_k = \left(\frac{Ra_e}{L^3}\right)^{1/3}$ , where  $Ra_e = \frac{\varepsilon E^2 L^2 \Delta \sigma}{4\nu D_s \rho \langle \sigma \rangle}$  is an electric Rayleigh number (see Baygents and Baldessari (1998)) and  $L$  is a characteristic large scale. While in stratified turbulence where  $\beta = 0$  and  $M = N = -f_{VB}$ ,  $k_k = \left(\frac{f_{VB}^2}{4\nu D_s}\right)^{1/4} \sim Ra^{1/4} L^{-1}$ , where  $Ra = \frac{gL^4}{\langle \rho \rangle \nu D_s} \left| \frac{d\rho_0}{dz} \right|$  is Rayleigh number. Note, at  $\beta = 0$ ,  $k_k$  is a virtual length scale since the CEF subrange has no intersection with the dissipation subrange.

### 3.3 Influence of the $i$ th solution

Eq. (3.1) is a third-order equation of  $u_{k,i}$ , there are three solutions in total, including one real solution and two complex solutions. In the investigation of Alam et al (2019), they solved the fifth-order equation (Eq. (4.2) in their paper) and only kept the real solution. However, as explained above, when we think about  $E_u = k^{-1}(u_k \cdot u_k^*)$ , complex solution of  $u_k$  can also lead to real  $E_u$ . Thus, it is necessary to revisit the roles of complex solution of  $u_k$  in the turbulent transport. It should be noted that, the Eq. (4.2) in Alam et al (2019) has 5 solutions with only three of them being independent. The independent solutions in their investigation are exactly the same as our prediction with Eq. (3.1). Eq. (4.2) in Alam et al (2019) is a specific case of Eq. (3.1) at  $\beta = 0$ .

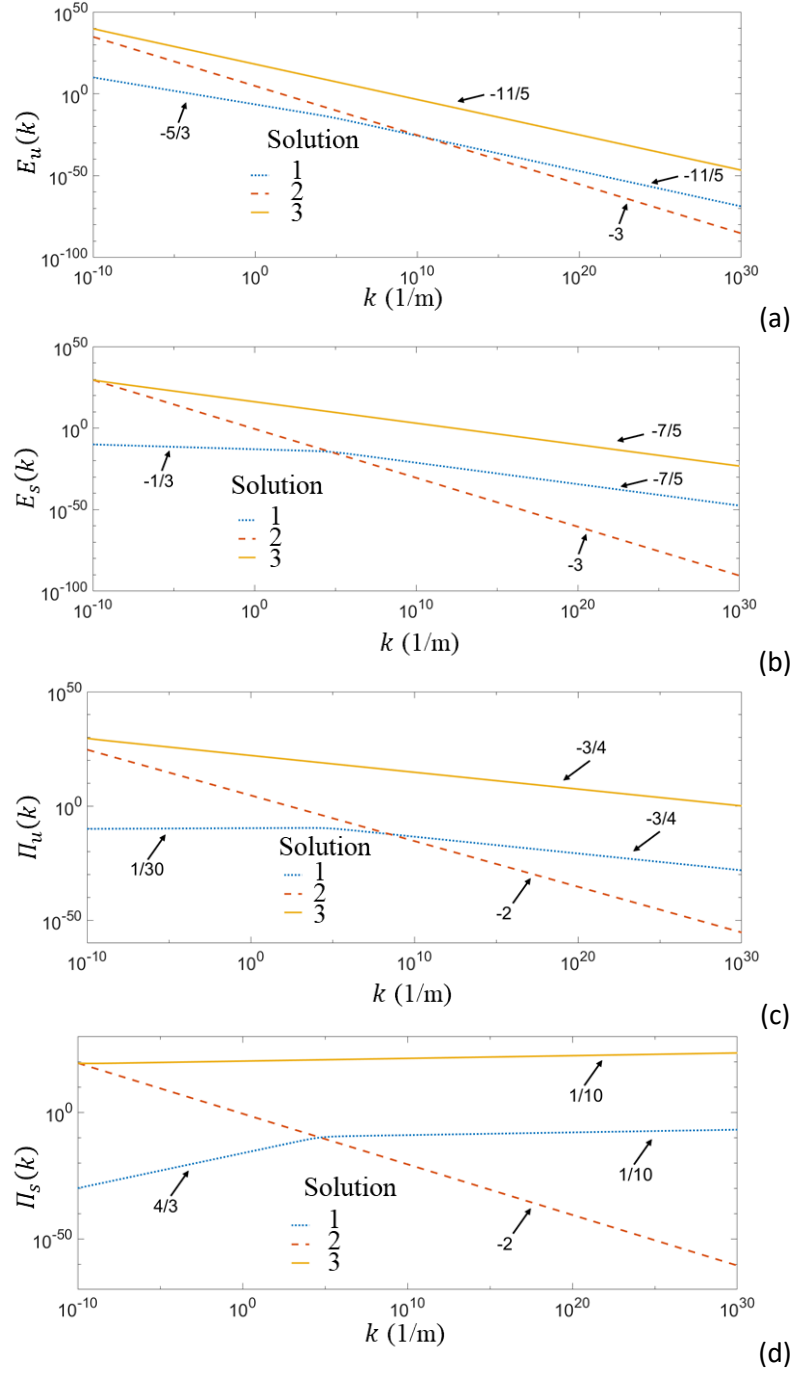


Figure 6 Influence of the  $i$ th solution, where  $M = N = 1$ ,  $\beta = 0$ . (a) Power spectra of kinetic energy  $E_u$ . Each curve has been shifted by  $10^5$  vertically. (b) Power spectra of scalar variance  $E_s$ . (c) Flux of kinetic energy  $\Pi_u$ . Each curve has been shifted by  $10^5$  vertically. (d) Flux of scalar variance  $\Pi_s$ .

Figure 6 shows the results at  $\beta = 0$ . From Figure 6(a), it can be seen there is no CEF subrange found in the VFD subrange, for the 2<sup>nd</sup> and 3<sup>rd</sup> solutions. In the entire wavenumber range, the 2<sup>nd</sup> and 3<sup>rd</sup> solutions lead to  $\xi_u = -3$  and  $\xi_u = -11/5$  respectively. The corresponding  $\xi_s$  are -3 and -7/5 respectively (see Figure 6(b)). For the 2<sup>nd</sup> solution, there is no constant flux of kinetic energy and scalar variance. The scaling exponents  $\lambda_u$  and  $\lambda_s$  are both -2, as can be found in Figure 6(c, d). While for the 3<sup>rd</sup> solution,  $\lambda_u = -3/4$  and  $\lambda_s = 1/10$ . The 3<sup>rd</sup> solution is equivalent to having a CSF subrange in the VFD subrange.

In contrast, when  $\beta = 2$ , from the 2<sup>nd</sup> and 3<sup>rd</sup> solutions, there are only CEF subrange found where  $\xi_u = -5/3$  and  $\xi_s = -13/3$ , as can be seen from Figure 7(a, b). The scaling exponents  $\lambda_u$  and  $\lambda_s$  are both 1/30 (i.e. approximately zero) and -8/3 (Figure 7(c, d)), respectively.

The investigations on the additional solutions show some unpredicted results that can be attributed to some bifurcation in the solution space. For instance, in stratified turbulence ( $\beta = 0$ ) in the atmosphere, -3 slope of kinetic energy spectra has been experimentally observed by Nastrom and Gage (Nastrom, Gage et al. 1984, Nastrom and Gage 1985) on synoptic scale, attributed. A later investigation by numerical simulation (Kitamura and Matsuda 2006) shows both the spectra of kinetic energy and potential energy (equivalent to density variance) have -3 slopes. The researchers focus on how the -3 spectra are generated (e.g. upscale or downscale cascade), but does not explain why there should be -3 spectra intrinsically. This investigation indicates the -3 spectra of kinetic energy and scalar variance are direct consequence of an inherent solution of the conservation equation (Eq. (2.15) or (3.1)). It must appear if some transitional conditions are satisfied.

#### 4. Discussions

To this end, we can answer the conjecture advanced in the introduction that there do exist symmetric cascade processes, with either constant or nonconstant fluxes of kinetic energy and scalar variance, if only the real solution of Eq. (2.15) is considered. The results are summarized in Table 1.

Table 1. Symmetry of cascade processes in forced turbulence

Subrange	Features	
	$\Pi_u$	$\Pi_s$
Inertial	Constant	Constant
CEF	Quasi-constant	Non-constant
CSF	Non-constant	Quasi-constant
Dissipation	Non-constant	Non-constant

Unfortunately, such symmetry of cascade was not found in the other two solutions. The symmetry is broken due to some unknown reason. For the 2<sup>nd</sup> solution, when  $\beta < 2/3$ , there is no CEF subrange. Instead, what we have is a new subrange (2<sup>nd</sup> solution) with non-constant  $\Pi_u$  and  $\Pi_s$ . The slopes of  $E_u$  and  $E_s$  are both -3. However, when  $2/3 < \beta < 4$ , there is only the CEF subrange observed in the entire computational region.

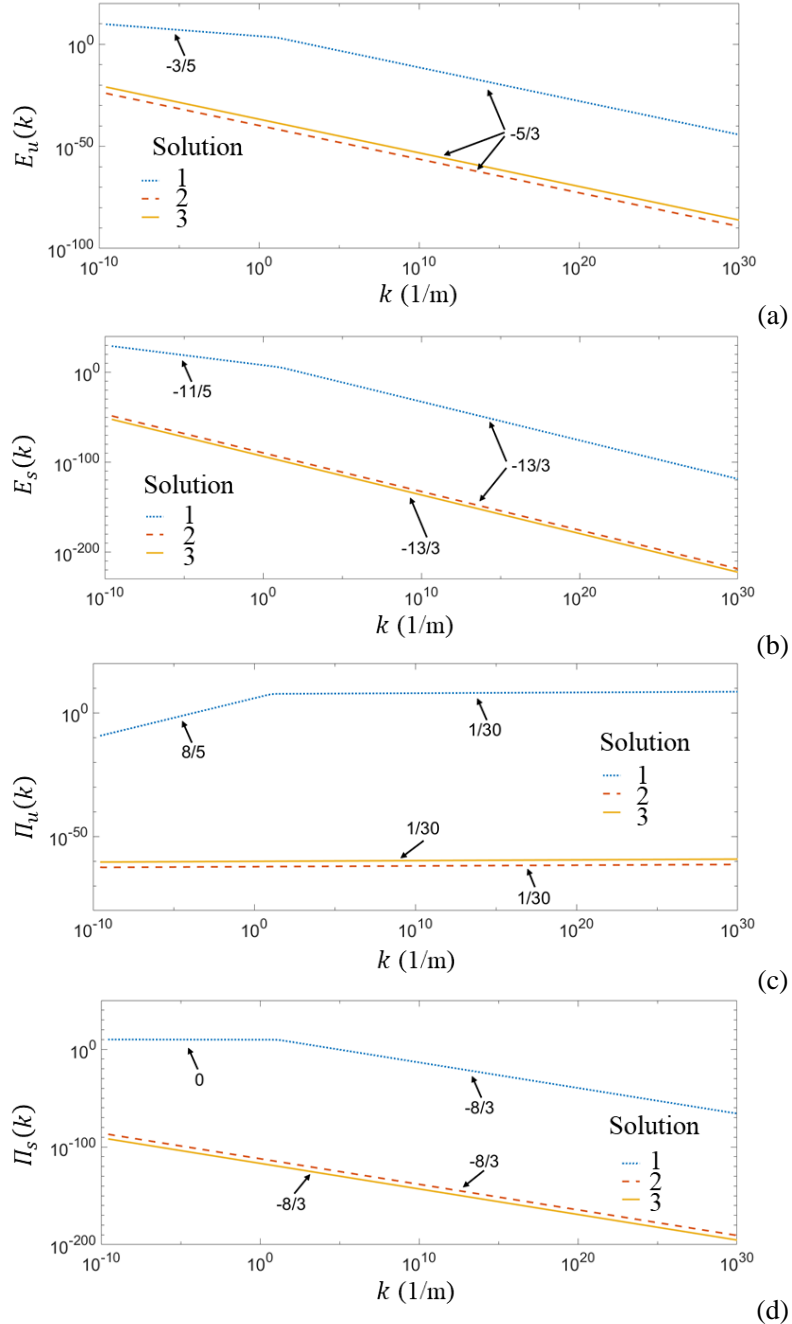


Figure 7 Influence of the  $i$ th solution, where  $M = N = 1$ ,  $\beta = 2$ . (a) Power spectra of kinetic energy  $E_u$ . Each curve has been shifted by  $10^5$  vertically. (b) Power spectra of scalar variance  $E_s$ . (c) Flux of kinetic energy  $\Pi_u$ . Each curve has been shifted by  $10^5$  vertically. (d) Flux of scalar variance  $\Pi_s$ .

In contrast, for the 3<sup>rd</sup> solution, we observe there is only the CEF subrange in the range  $0 \leq \beta \leq 2.657$ . When  $2.657 < \beta < 4$ , we observe astonishing ascending  $\Pi_u$  and  $\Pi_s$  with their slopes highly positive. For instance, at  $\beta = 3$  and  $4$ ,  $\lambda_u = 10.5$  and  $16$ , and  $\lambda_s = 14.5$

and 20 respectively. The surprising large slopes of  $\Pi_u$  and  $\Pi_s$  is weird and impractical, if the scalar variance cascades from lower to higher wavenumbers. Accordingly, we may ignore the 3<sup>rd</sup> solution in the range  $2.657 < \beta < 4$ .

The example of existing -3 slopes in  $E_u$  and  $E_s$  at  $\beta = 0$  implies the 2<sup>nd</sup> and 3<sup>rd</sup> solutions could be realized in nature and engineering under some conditions, which require more investigations.

In this investigation, defining the property of  $\beta$  is difficult. From the spectral format of Eq. (2.4c), it seems appropriate to define  $\beta$  as any real number smaller than 4, including the fractional number and even negative number if physically appropriate. It is unable to answer this question here and we hope to leave it for future research. Applying real  $\beta$  provides an effective tool to classify the turbulence driven by scalar-based volume force, since the same or close  $\beta$  in different turbulent systems reserve the same or similar transport process of kinetic energy and scalar variance. Therefore, instead of seeking the solution of each type of turbulence, researchers can numerically solve the conceptual model in Eqs. (2.1a-c) with  $\beta$  for general solutions, e.g. under specific boundary conditions.

## 5. Conclusions

In this investigation, we numerically studied the transport of kinetic energy and scalar variance in turbulence driven by scalar-based volume force. In this type of turbulence, the scalar field is strongly coupled with the velocity field and dominated by active transport. A conservative equation relying on the fluxes of kinetic energy and scalar variance has been established. The equation has three solutions, one real solution and two complex solutions. Based on the solutions, a comprehensive cascade picture has been established for this type of turbulence.

The investigations on the real solution indicate the turbulence have symmetric cascade processes, including inertial subrange (constant fluxes of kinetic energy and scalar variance), CEF subrange (quasi-constant flux of kinetic energy), CSF subrange (quasi-constant flux of scalar variance), and dissipation subrange (nonconstant fluxes of kinetic energy and scalar variance). The scaling exponents in the power spectra of kinetic energy and scalar variance strictly depend on the order of derivatives, i.e.  $\beta$ . In the CEF subrange,  $\xi_u$  is always  $-5/3$ , while  $\xi_s = -(6\beta + 1)/3$  which has never been reported. In the CSF subrange,  $\xi_u = (4\beta - 11)/5$  and  $\xi_s = -(2\beta + 7)/5$  which are both consistent with the theory of Zhao and Wang (Zhao and Wang 2021). When  $\beta < 2/3$ , the CEF subrange locates on the lower wavenumber side of the CSF subrange. When  $\beta > 2/3$ , the CEF subrange locates on the higher wavenumber side of the CSF subrange. We also examined the influence of  $MN$  and the initial value of the real solution  $u_{k,1,1}$  on the critical wavenumber between CEF and CSF subranges. As  $\beta$  is increased,  $k_{ci}$  first increases with  $MN$ , and then decreases with  $MN$ , following a power-law relationship. In contrast, as  $\beta$  is increased,  $k_{ci}$  first decreases with  $u_{k,1,1}$ , and then increases with  $u_{k,1,1}$  with power-law relationship. Another microscale, which could be the smallest length scale in this type of turbulence, is also theoretically investigated. The result indicates  $k_k = \left(\frac{MN}{4\nu D_s}\right)^{\frac{1}{4-\beta}}$ , which prevents  $\beta$  to be equal or larger than 4.

A further investigation on the 2<sup>nd</sup> solution (a complex solution) of the conservative equations shows the symmetry of the cascade process is broken. When  $\beta < 2/3$ , we only observe a new subrange with non-constant  $\Pi_u$  and  $\Pi_s$ , where  $\xi_u = \xi_s = -3$ . However, when  $2/3 < \beta < 4$ , only the CEF subrange is present. For the 3<sup>rd</sup> solution (another complex

solution), there is only the CEF subrange in the range  $0 \leq \beta \leq 2.657$ . Beyond this range, the 3<sup>rd</sup> solution becomes physically inappropriate.

This paper aims to establish a comprehensive picture of the cascade process in forced turbulence and the accompanied active transport process, within a unified theoretical frame. In the meanwhile, we hope this investigation can significantly deepen our understanding of the transport of kinetic energy and scalar variance, e.g. in stratified turbulence, electrokinetic turbulence and other physical systems like condensed matter physics. The scalar is not restricted to any known physical quantities, e.g. temperature, density, electric conductivity and permittivity etc, but also includes broad scalar quantities like information.

**Acknowledgement** The investigation is supported by the National Nature Science Foundation No. 11672229.

## 6. References

Alam, S., A. Guha and M. K. Verma (2019). "Revisiting Bolgiano–Obukhov scaling for moderately stably stratified turbulence." *Journal of Fluid Mechanics* **875**: 961-973.

Baygents, J. C. and F. Baldessari (1998). "Electrohydrodynamic instability in a thin fluid layer with an electrical conductivity gradient." *Physics of fluids* **10**(1): 301-311.

Benzi, R., L. Biferale, S. Ciliberto, M. V. Struglia and R. Tripiccione (1996). "Generalized scaling in fully developed turbulence." *Physica D* **96**: 162-181.

Bolgiano, R. (1959). "Turbulent spectra in a stably stratified atmosphere." *Journal of Geophysical Research* **64**(12): 2226-2229.

Corrsin, S. (1951). "On the Spectrum of Isotropic Temperature Fluctuations in an Isotropic Turbulence." *Journal of Applied Physics* **22**(4): 469-473.

Davidson, P. A. (2013). *Turbulence in Rotating, Stratified and Electrically Conducting Fluids*. New York, Cambridge University Press.

Frisch, U. (1995). *Turbulence—The legacy of A. N. Kolmogorov*. New York, USA, Cambridge University Press.

Howland, C. J., J. R. Taylor and C. P. Caulfield (2020). "Mixing in forced stratified turbulence and its dependence on large-scale forcing." *Journal of Fluid Mechanics* **898**: A7.

Kitamura, Y. and Y. Matsuda (2006). "The  $k_H^{-3}$  and  $k_H^{-5/3}$  energy spectra in stratified turbulence." *Geophysical Research Letters* **33**: L0580.

Kolmogorov, A. N. (1941). "The Local Structure of Turbulence in Incompressible Viscous Fluid for Very Large Reynolds Numbers." *Doklady Akademii Nauk SSSR* **30**(4): 301-304.

Lohse, D. and K.-Q. Xia (2010). "Small-Scale Properties of Turbulent Rayleigh-Bénard Convection." *Annual Review of Fluid Mechanics* **42**: 335-364.

Maffioli, A. and P. A. Davidson (2016). "Dynamics of stratified turbulence decaying from a high buoyancy Reynolds number." *Journal of Fluid Mechanics* **786**: 210-233.

Nastrom, G. D. and K. S. Gage (1985). "A climatology of atmospheric wavenumber spectra of wind and temperature observed by commercial aircraft." *Journal of the Atmospheric Sciences* **42**: 950 – 960.

Nastrom, G. D., K. S. Gage and W. H. Jasperson (1984). "The atmospheric kinetic energy

spectrum,  $10^0 - 10^4$  km." Nature **310**: 36-38.

Niemela, J. J., L. Skrbek, K. R. Sreenivasan and R. J. Donnelly (2000). "Turbulent convection at very high Rayleigh numbers." Nature **404**: 837-840.

Obukhov, A. M. (1949). "Structure of the temperature field in turbulent flow." Izv. Akad. Nauk. SSSR, Ser. Geogr. and Geophys **13**(1): 58-67.

Obukhov, A. M. (1959). "The influence of hydrostatic forces on the structure of the temperature field in turbulent flow (English translation)." Dokl. Acad. Sci. USSR, Earth Sci. Sect **125**: 1246-1248.

Okino, S. and H. Hanazaki (2020). "Direct numerical simulation of turbulence in a salt-stratified fluid." Journal of Fluid Mechanics **891**: A19.

Verma, M. K. (2004). "Statistical theory of magnetohydrodynamic turbulence: recent results." Physics Reports **401**(5): 229-380.

Verma, M. K. (2018). Physics of Buoyancy Flows: From Instabilities to Turbulence. New Jersey, World Scientific.

Wang, G., F. Yang and W. Zhao (2014). "There can be turbulence in microfluidics at low Reynolds number." Lab on a Chip **14**(8): 1452 - 1458.

Wang, G., F. Yang and W. Zhao (2016). "Microelectrokinetic turbulence in microfluidics at low Reynolds number." Physical Review E **93**: 013106.

Zhao, W. and G. Wang (2017). "Scaling of velocity and scalar structure functions in ac electrokinetic turbulence." Physical Review E **95**: 023111.

Zhao, W. and G. Wang (2019). "Cascade of turbulent energy and scalar variance in DC electrokinetic turbulence." Physica D **399**: 42-50.

Zhao, W. and G. Wang (2021). "A tentative study of the transport of energy and other scalar quantities in forced turbulence driven by  $\nabla^n A$ -type volume forces." Journal of Hydrodynamics **33**(6): 1271-1281.